Liquefaction Ground Deformations and Cascading Coastal Flood Hazard in the 2023 Kahramanmaraş Earthquake Sequence

Patrick Bassal,[1)] M.EERI, Elena Papageorgiou,[2-3)] Diane M. Moug,[4)] M.EERI, Jonathan D. Bray,[5)] M.EERI, K. Onder Cetin,[6)] Arda Şahin,[7)] Ethan J. Kubatko,[a)] Suranjan Nepal,[a)] Charles Toth,[a)] Sena B. Kendır,[8)] Murat Bikçe[9)]

The 2023 Kahramanmaraş earthquake sequence produced extensive liquefaction-induced ground deformations and ongoing flooding along the shoreline of the Mediterranean port city of İskenderun, Türkiye. This study compiles field observations and analyses from cross-disciplinary perspectives to investigate whether earthquake-induced liquefaction was a significant factor for increasing the flood hazard in İskenderun. Geotechnical reconnaissance observations following the earthquakes included seaward lateral spreading, settlement beneath buildings, and failures of coastal infrastructure. Three presented lateral spreading case histories indicate consistent ground deformation patterns with areas of reclaimed land. Persistent Scatterer Interferometry (PSI) measurements from Synthetic Aperture Radar (SAR) imagery identify a noticeably greater rate of pre- and post-earthquake subsidence within the İskenderun coastal and urban areas relative to surrounding regions. The PSI measurements also indicate subsidence rates accelerated following the earthquakes and were typically highest near observed liquefaction manifestations. These evaluations suggest that while the liquefaction of coastal reclaimed fill caused significant ground deformations in the shoreline area, ongoing subsidence of İskenderun and other factors likely also exacerbated the flood hazard. Insights from this work suggest the importance of evaluating multi-hazard liquefaction and flood consequences for enhancing the resilience of coastal cities.

INTRODUCTION

On February 6, 2023, the moment magnitude (M_w) 7.8 mainshock of the Kahramanmaraş earthquake sequence caused widespread liquefaction-induced ground deformations along the

[1)] The Ohio State University, Department of Civil, Environmental, and Geodetic Engineering, OH 43210, USA
[2)] Aristotle University of Thessaloniki, Department of Physical & Environmental Geography, 54124 Thessaloniki, Greece
[3)] Center for Interdisciplinary Research and Innovation (CIRI-AUTH), Balkan Center, 57001 Thermi, Greece
[4)] Portland State University, Department of Civil and Environmental Engineering, OR 97201, USA
[5)] University of California, Civil and Environmental Engineering Department, Berkeley, CA 94720, USA
[6)] Middle East Technical University, Civil Engineering Department, 06800 Ankara, TR
[7)] University of California, Civil and Environmental Engineering Department, Los Angeles, CA 90095, USA
[8)] Zemın Etüd ve Tasarim A.Ş., 34794 İstanbul, TR
[9)] İskenderun Technical University, Civil Engineering Department, 31200 İskenderun, TR

Corresponding author:
Patrick Bassal, The Ohio State University, Department of Civil, Environmental, and Geodetic Engineering, 2036 Neil Avenue, Columbus, OH 43210, USA, email: bassal.3@osu.edu

coast of the Mediterranean port city of İskenderun, Hatay Province, Türkiye. Several reconnaissance teams, including the Middle East Technical University (METU), Geotechnical Extreme Events Reconnaissance (GEER) Association, and Earthquake Engineering Research Institute (EERI), performed field investigations to document the damage and collect perishable data soon after the earthquakes (METU 2023, Cetin et al. 2023, Moug et al. 2023). Observed liquefaction effects in İskenderun included widespread sediment ejecta, ground and building settlement, seaward lateral spreading, and damage to shoreline protection structures. Additionally, coastal flooding during storms and high tide events inundates large portions of the city more frequently since the earthquakes occurred.

Soil liquefaction in low-lying coastal areas is postulated as an important contributor to increased flood hazard following several past earthquakes. Dramatic subsidence and loss of land to the sea within coastal areas in the 1964 Great Alaska, 1992 Flores Island Indonesia, and 1999 Kocaeli earthquakes are associated with subsurface liquefaction and lateral spreading (e.g., Lemke 1966, Ishihara 2003, Cetin et al. 2004). Floodplain subsidence due to liquefaction in the 2010-2011 Canterbury Earthquake Sequence in New Zealand similarly increased the severity of coastal inundation and inland flood hazards (e.g., Hughes et al. 2015, Davis et al. 2015). Paleoseismic studies along the Cascadia Subduction Zone in the northwestern United States indicate past cycles of coseismic coastal submergence influenced by both regional tectonic movements, as well as local settlement within organic and liquefiable soil deposits (e.g., Atwater 1987, Darienzo and Peterson 1990). Insights from additional well-documented case studies can help distinguish the role of liquefaction-induced ground deformations relative to other factors for the post-earthquake flood hazard.

This paper expands on insights by Moug et al. (2023) with additional field observations and remote sensing evaluations, to help elucidate whether soil liquefaction was a primary contributor to post-earthquake coastal flooding in İskenderun. First, the geologic and historical setting, earthquake events, and available subsurface data are discussed. Post-earthquake field observations of flooding and liquefaction ground deformations, including case studies of shoreline lateral spreading, are next detailed. Persistent Scatterer Interferometry (PSI) measurements from Synthetic Aperture Radar (SAR) imagery is used to detect spatial patterns of ground movement relative to the field data. General insights from these observations and the liquefaction-flood relationship in İskenderun are discussed.

LOCAL GEOLOGY AND RECENT DEVELOPMENT

İskenderun is located within a low-lying alluvial floodplain east of the Nur mountains, along the gulf of İskenderun within the eastern Mediterranean Sea. The gulf has a typical water depth of less than 70 m and overlies the İskenderun basin (Aksu et al. 1992). Quaternary-age alluvium extends to depths of 2000 m at the southwest edge of the basin, but thins considerably (e.g., < 500 m) to the northeast of the basin near İskenderun (Aksu et al. 2005). The thickness of Quaternary alluvium in the İskenderun region is approximated as 35-40 m from geophysical surveys by Ozdemir et al. (2019), and is composed of heterogenous gravels, sands, silts, and clays that become less gravelly near the shoreline (Orukoğlu and İşhani 2010).

Figure 1. Historical map of İskenderun dated 1916 [obtained from the National Library of Turkey by Nalça (2018)].

A shallow water table and an abundance of marshes slowed the development of İskenderun (formerly known as Alexendretta) under Ottoman rule in the 19th century (Nalça Kıssaboylu et al. 2023). A historic 1916 map (Figure 1) obtained from the National Library of Turkey by Nalça (2018) depicts the early swamps and marshes, built areas, and shoreline near the end of the Ottoman era. The İbrahim Paşa channel indicated in Figures 1 and 2 was constructed in the 1830's to drain the marshes and swamps. However, it was poorly maintained and gradually filled with sediment deposits. Under the French Mandate period from 1919 to 1939, the placement of fill and construction of more robust concrete drainage

channels improved the land for development. Urban improvements included the construction of present-day Atatürk Boulevard. Following this time, İskenderun continued to develop and experienced another resurgence in growth as factories were built in the 1970's.

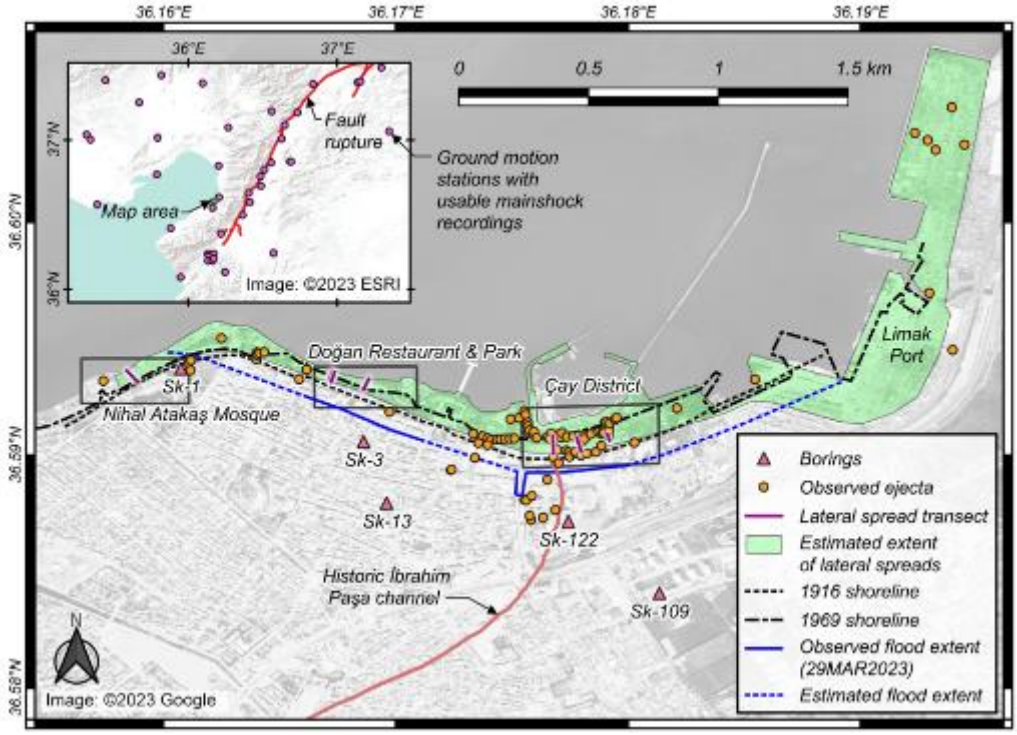

Figure 2. Map of approximate early shoreline extents, borings, and post-earthquake observations in İskenderun [map images ©2023 ESRI and ©2023 Google].

The İskenderun shoreline was built out during the city's development. The 1916 shoreline depicted in Figure 1 approximately aligns with present-day Atatürk Boulevard. It represents the approximate border between reclaimed and naturally formed land. A satellite image of İskenderun in 1969 presented by Taftsoglou et al. (2023) shows reclaimed land built out beyond the 1916 shoreline but typically short of the present-day shoreline. These sources indicate the extent of shoreline filling just prior to the French Mandate period, and just prior to the 1970's industrialization. The 1916 and 1969 historic shoreline extents and location of the İbrahim Paşa channel are traced with post-earthquake observations in Figure 2. These provide a basis to delineate potential subsurface constraints on the extent of liquefaction and lateral spreading.

İskenderun has been affected by several historic earthquake events (Ambraseys 1989). On August 13, 1822, the ~M_w 7.5 Aafrine earthquake destroyed several houses and caused widespread liquefaction along the coast. Liquefaction also presumably caused the water to

rise and inundate several settlements within cultivated lands at the base of the present-day Nur mountains. The ~M_w 7.2 Amik Gölü earthquake on April 3, 1872 also damaged settlements in İskenderun, although the extent of damage has not been well documented.

THE 2023 KAHRAMANMARAŞ EARTHQUAKE SEQUENCE

The Kahramanmaraş earthquake sequence was comprised of a M_w 7.8 mainshock in the Pazarcık area of Kahramanmaraş on February 6, 2023 at 4:17 am local time, and a M_w 7.7 aftershock nine hours later located in the Elbistan District of Kahramanmaraş. Several other aftershocks occurred, including a M_w 6.4 event in the Hatay region on February 20 that was also felt in İskenderun. The earthquakes exhibited primarily strike-slip faulting within the East Anatolian Fault zone, along a triple junction between the Anatolia, Arabian, and African tectonic plates (Goldberg et al. 2023). The city of İskenderun is located approximately 19 km to the west of the East Anatolian fault rupture (Reitman et al. 2023) and was predominantly affected by the mainshock.

Recordings from nearby ground motion stations were processed and compiled by Buckreis et al. (2023). The fault rupture and nearby usable recording stations following the mainshock are indicated in the inset map of Figure 2. Turkish National Strong Motion Network stations TK3115 (~4 km northwest of the urban area) and TK3116 (~5 km south of the İskenderun urban area) recorded horizontal geomean peak ground accelerations (PGAs) of 0.28 g and 0.17 g during the mainshock. Additionally, station TK3112 located within 2 km of the urban area recorded the initial portion of shaking but terminated following a horizontal acceleration spike of under 0.20 g for unknown reasons during the mainshock. Stations TK3112, TK3115, and TK3116 recorded horizontal geomean PGAs of 0.07 g, 0.11 g, and 0.03 g during the February 20 aftershock. Significantly lower PGAs were recorded during the M_w 7.7 February 6 aftershock. The shear wave velocity in the upper 30 m (V_{s30}) was measured as 233 m/s, 424 m/s, and 870 m/s at TK3112, TK3115, and TK3116, respectively, as corrected by Buckreis et al. (2023) using data from the Disaster Management and Emergency Authority in Türkiye. Stations TK3112 and TK3116 are in an area of undifferentiated quaternary sediments, and TK3115 is in an area of clastic and carbonate rocks, according to the 1:500,000 scale geologic map by Utu et al. (2002). Inspections of these stations on March 2 and March 3, 2023 by Cetin et al. (2023) noted liquefaction-induced sediment ejecta within 100 m of TK3112, however, no obvious ground deformations were observed near TK3115 and TK3116.

Synthetic aperture radar (SAR) was used by Goldberg et al. (2023) and Mai et al. (2023) to delineate the fault rupture and estimate three-dimensional coseismic surface displacements of the affected region. These studies performed subpixel offset tracking of pre- and post-earthquake Sentinel-1 SAR image pairs from multiple orbits. The maps developed by Mai et al. (2023) identify large left-lateral surface fault offsets (exceeding 4 m near the rupture) but suggest much smaller vertical displacements due to the strike-slip mechanism. Negligible movements are indicated by these studies in İskenderun, possibly due to low coherency between image pairs within the liquefaction-affected urban area (e.g., Chatzipetros et al. 2021). Nonetheless, these studies may suggest an insignificant amount of subsidence caused by vertical tectonic movements in İskenderun. Additionally, no Global Navigation Satellite System (GNSS) recordings are available within İskenderun to evaluate potential deviations of local subsidence relative to general tectonic movements. Alternative datasets and methods are considered in this study to approximate localized movements within İskenderun.

SUBSURFACE CONDITIONS

A geophysical and geotechnical site investigation program was performed as part of a city-wide seismic microzonation study in İskenderun (Orukoğlu and İşhani 2010). That study included a series of 148 borings drilled in the spring of 2010 to depths of 6-30 m at approximately 500 m x 500 m gridded intervals, with intermittent standard penetration tests (SPTs) and samples obtained for index testing. Groundwater was observed in several of those borings, indicating a groundwater depth of 1-3 m beneath the ground surface within the urban and shoreline areas.

Five representative borings, which are labeled Sk-1, -3, -13, -109, and -122 in Figure 2, are depicted in Figure 3. The logs indicate the uncorrected SPT blow count over 30 cm (N), the fines content (FC; percent soil by mass passing a 0.075 mm sieve), the plasticity index (PI), and a layer description with the soil classification, color, and consistency. Energy calibrations and other hammer details are unavailable for these borings, such that the N-values cannot be reliably adjusted to perform liquefaction triggering assessments. The soil classification provided in the boring logs by Orukoğlu and İşhani (2010) does not indicate strict adherence to a common convention. The group names were corrected in Figure 3 at layers with available FC and PI data, such that they better adhere to the unified soil classification system (USCS). However, the absence of details to inform the gradation of the sands and gravels prevent full adherence to a USCS group name.

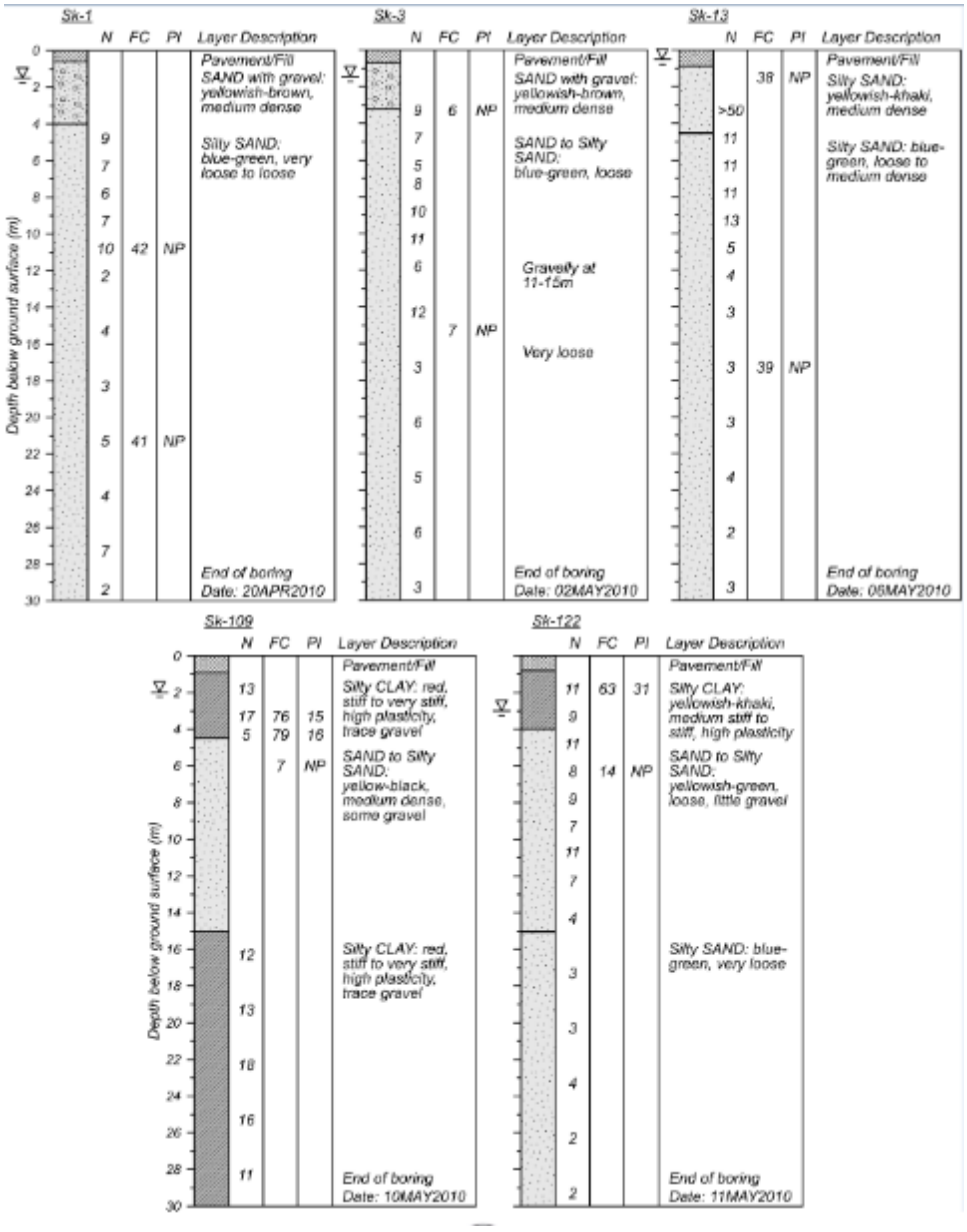

Figure 3. Logged data from five 30 m deep borings in İskenderun [modified from Orukoğlu and İşhani (2010)].

Borings Sk-1, -3, and -13 located in the western part of the urban area indicate relatively similar soil conditions with a 3-5 m medium dense layer of gravelly to silty sand, underlain by a thick deposit of very loose to medium dense silty sand and sand to the maximum depth explored of 30 m. Borings Sk-122 (i.e., in the Çay District) and Sk-109 (i.e., about 500 m southeast of Sk-122) each indicate a top layer of 4-5 m stiff silty clay of high plasticity (i.e., PI >15). Boring Sk-122 indicates loose silty sand from a depth of 4 m to 15 m and very loose silty sand from a depth of 15 m to at least 30 m. Boring Sk-109 indicates medium dense silty

sand from a depth of 4.5 m to 15 m, and stiff to very stiff silty clay from a depth of 15 m to at least 30 m.

The general liquefaction triggering potential of subsurface soils in İskenderun can be roughly estimated for the M_w 7.8 mainshock. Assuming a geomean PGA of 0.28 g as recorded at soil site TK3115, a groundwater depth of 2 m, and unit weights of 17 kN/m^3 and 18 kN/m^3 above and below the groundwater table, respectively, results in an adjusted cyclic stress ratio (i.e., CSR, adjusted to an equivalent earthquake magnitude of M=7.5 and vertical effective stress of 1 atm) of 0.25 to 0.28 for depths of 4 to 6 m per Boulanger and Idriss (2015). This assumes no site amplification, which may underestimate the actual PGA at soft soil sites that liquefied. A clean-sand corrected SPT blow count adjusted to an equivalent energy ratio of 60% and vertical effective stress of 1 atm [$(N_1)_{60cs}$] of about 20 to 24 would be necessary for a probability of liquefaction triggering of 50% (i.e., considering empirical model uncertainty) per Boulanger and Idriss (2012). The $(N_1)_{60cs}$ depends on an overburden correction factor (i.e., C_N; a multiplicative factor of about 1.3 to 1.5 for the example depth range of 4 to 6 m), a clean sand adjustment [i.e., $\Delta(N_1)_{60}$; an additive factor ranging from 0 blows for clean sands (FC < 5%) to 5.5 blows for highly silty sands (FC > 35%)], and hammer energy corrections that are not known for the available data. Assuming no bias due to hammer energy, liquefaction likely triggered in the low blow count sands and silty sands in the Figure 3 borings. In combination with the ground observations of liquefaction, these estimates help to confirm that liquefaction occurred within sands and silty sands during the M_w 7.8 mainshock in İskenderun.

None of the borings by Orukoğlu and İşhani (2010) nor geophysical surveys by Orukoğlu and İşhani (2010) and Ozdemir et al. (2019) were performed seaward of the 1916 shoreline, and thus preclude a detailed characterization of the coastal reclaimed fill. Soil boring data from local sources near the Nihal Atakaş mosque area (e.g., Ozener et al. 2024) depict general consistency in soil strata and SPT blow counts with the nearest inland boring presented herein (i.e., Sk-1). Work is currently ongoing to collect additional detailed subsurface data, including seismic cone penetration tests and soil borings, at several case history sites affected by liquefaction These additional data will enable more reliable evaluations of liquefaction triggering and liquefaction-induced ground deformations.

POST-EARTHQUAKE FIELD OBSERVATIONS

Liquefaction and lateral spreading

Post-earthquake observations of perishable liquefaction effects in İskenderun were well documented by reconnaissance teams following the earthquakes (e.g., METU 2023, Cetin et al. 2023, Moug et al. 2023). Figure 2 indicates locations of liquefaction-induced sediment ejecta indicated by the field teams soon after the earthquake events. These field observations indicate liquefaction occurred primarily in the reclaimed shoreline areas (e.g., post-1916 fills), but was also observed inland of the 1916 shoreline in the Çay District. Due to limited time to perform post-earthquake surveys in İskenderun, these points may not be inclusive of all instances of sediment ejecta. A total of 22 buildings in İskenderun were surveyed by Moug et al. (2023), with liquefaction-induced settlements ranging from negligible to over 70 cm. These are further detailed by Moug et al. (2024; in this special issue). Damage to coastal facilities following the earthquakes included the partial collapse of a pile-supported naval base wharf, extensional displacements along pier and jetty structures, and the settlement of armor stones of the rubble mound seawall along much of the shoreline by 50-100 cm.

Several instances of lateral spreading ground displacements along the İskenderun shoreline were recorded by reconnaissance teams following the February 6 earthquakes (e.g., METU 2023, Cetin et al. 2023, Moug et al. 2023). Lateral spreading manifests as translational ground movement and is commonly attributed to shearing along subsurface liquefied soils in areas with gently sloping ground or near a free face. Field observations of lateral spreading extended from the western shoreline of İskenderun to the Limak Port at the northeast of İskenderun, as mapped in Figure 2. Instances of shoreline lateral spreading were also documented at least as far north as the city of Dörtyol (e.g., Cetin et al. 2023), and likely occurred to the south of İskenderun as observed from post-earthquake satellite imagery (e.g., Taftsoglou et al. 2023).

Post-earthquake flooding

Images circulating over the news and social media indicated coastal flooding in İskenderun on February 6, 2023 soon after the M_w 7.8 mainshock (e.g., Soylu 2023). Although the initial flood waters dissipated shortly after, residents of İskenderun reported unusually frequent flooding over the weeks following the earthquakes. The increased flood hazard was summarized by a long-term local resident and building owner who corresponded with the GEER team on August 29, 2023:

"*Before the quake, we used to get one flooding every couple of years at most. Mainly if it rained too heavily too quickly or too long where the pumping stations were overwhelmed. But now as the coastal area [near the Çay District] has dropped lower compared to sea, it is more frequent. Almost all the time when the tide is high, or alternatively if the sea is choppy and northerly winds are blowing, we get flooding.*"

Figure 4. Flooding in İskenderun on March 29, 2023 along (a) Mareşal Fevzi Çakmak Street in the Yenişehir District, over 250 m from the shoreline (36.5912N, 36.1698E), and (b-c) Bahçeli Sahil Evler Street in the Çay District (36.5910N, 36.1792E), where water was observed expelling from a drain (36.5900N, 36.1768E).

The reports of flooding were consistent with observations by the GEER team of several building owners pumping water from their basements on March 28, 2023. The GEER team encountered notable flooding on March 29, 2023 (Figure 4). By the afternoon on this day, moderate rainfall and strong winds (i.e., reaching ~50 kmph due south, with higher gust speeds) impacted the İskenderun area. The nearest active tide station located in Arsuz indicated that the initiation of flooding aligned with the time at which the sea level was nearing high tide (VLIZ-IOC 2023). Waves were observed to overtop the existing seawall within the Yenişehir District. The flooding extended to over 250 m inland. The observed flood extents are indicated in Figure 2 (solid blue lines). The approximate flood extents in Figure 2 (dashed blue lines) were assumed from observations, discussions with locals, and drone coverage by local news reports (e.g., A Haber 2023). Flooding advanced at least two roads in from the shoreline, including past Mareşal Fevzi Çakmak Street (Figure 4a). The

coastal storm surge uplifted and displaced rubble mound stones from the seawall and caused the partial collapse of the Teysir restaurant located along the waterfront of the Yenişehir District (A Haber 2023). Along Bahçeli Sahil Evler Street in the Çay District (Figure 4b), water was observed to flow out of a storm drain cap (Figure 4c), likely due to a damaged water drainage system as reported by METU (2023). Such damages to drainage and water pumping systems likely reduced their performance and contributed to the sustained flooding conditions observed. When the team returned to İskenderun on April 1, 2023, flooding had largely diminished, but standing water remained in some locations.

LATERAL SPREADING CASE HISTORIES

Three case histories of lateral spreading are detailed herein at the following locations: (1) near the Nihal Atakaş mosque, (2) near the Doğan restaurant and Emekliler Park, and (3) within the Çay District. The three lateral spreading case histories include seven primary transects (i.e., LS-1 to -7) where detailed measurements of accumulated displacements were obtained by Moug et al. (2023). Lateral spreading distances along the transects were measured from the inside of the waterfront seawall or shoreline to all visible cracks along the transect path. The widths of the crack openings were measured and accumulated along each transect using the methodology of Robinson et al. (2010) to obtain seaward displacements. The transects were typically selected in areas where crack openings could be easily identified (e.g., near paved walkways, not obscured by vegetation).

All three lateral spreading case histories occurred at sites with primarily level ground. Average slopes across the lateral spreading transects measured from pre-earthquake surveys presented by Orukoğlu and İşhani (2010) are typically within 0.6° downward towards the seaward direction. Free face heights at the seaward extents of the lateral spreading transects were not directly measured in the field. Elevation differences across the shoreline structures (i.e., seawalls and wharves) near each transect are estimated to vary between 1.5 m and 5 m, based on 1916 bathymetric depths presented in the Figure 1 map. However, the 1916 map may not represent current conditions due to later construction works, dredging, natural depositional processes, and other shoreline activities. Upcoming site investigations intend to verify the free face height at these locations. Tables 1 and 2 present the date, start and end coordinates, length, ground slope, free face height and distance, and total accumulated lateral displacements for each transect. A transect representing building measurements adjacent to

LS-2 is also included in these tables (labeled LS-2′). Details regarding each lateral spreading case history site and associated transects are next presented.

Table 1. Coordinates of lateral spreading transects.

ID	Date	Start Coordinates		End Coordinates	
		Lat (N°)	Long (E°)	Lat (N°)	Long (E°)
LS-1	3/28/23	36.59362	36.15844	36.59314	36.15890
LS-2	4/1/23	36.59361	36.16726	36.59325	36.16712
LS-2′	4/1/23	36.59350	36.16720	36.59333	36.16714
LS-3	4/1/23	36.59357	36.16738	36.59315	36.16723
LS-4[a]	3/28/23 4/1/23	36.59327	36.16884	36.59283	36.16862
LS-5	4/1/23	36.59081	36.17677	36.59008	36.17679
LS-6	3/29/23	36.59072	36.17781	36.59016	36.17798
LS-7	4/1/23	36.59090	36.17911	36.59064	36.17921

[a] LS-4 was measured twice, before and after the March 29, 2023 storm.

Table 2. Measurements along and near lateral spreading transects.

ID	Date	Length (m)	Slope (°)[b]	Free face height (m)[c]	Free face dist. (m)[d]	Total lat. disp. (cm)
LS-1	3/28/23	65	0.1	1.5-3.5	0	54
LS-2	4/1/23	41	0.3	1.5-3.5	0	77
LS-2′	4/1/23	20	0.3	1.5-3.5	15	29
LS-3	4/1/23	45	0.3	1.5-3.5	0	73
LS-4[a]	3/28/23 4/1/23	52	0.2	2.5-5	0	0 147
LS-5	4/1/23	82	-0.3	1.5-4	67	53
LS-6	3/29/23	63	-0.4	1.5-4	100	27
LS-7	4/1/23	35	0.6	1.5-4	100	20

[a] LS-4 was measured twice, before and after the March 29, 2023 storm.

[b] Average ground slope across transect estimated from ground surveys presented by Orukoğlu and İşhani (2010); positive values indicate downward slope towards sea.

[c] Free face height range estimated from 1916 bathymetry depths (Figure 1) relative to current ground level.

[d] Free face distance is relative to start coordinates at seaward extent of transects.

Nihal Atakaş Mosque

The first lateral spreading case history site (36.5934N, 36.1584E) is located along the west shoreline of İskenderun, to the east of the Nihal Atakaş mosque, and near the Park Forbes AVM shopping mall as indicated in Figure 5. The mosque is partially built over reclaimed fill placed in 2016, as observed from satellite imagery (Maxar 2016). Following the earthquake, significant sediment ejecta covered an area of over 500 m^2 along the northeast corner of the mosque over the recent fill (Figure 6a). Several cracks parallel to the shoreline were observed between the seawall and Atatürk Boulevard (Figure 6b). The cracks and ejecta features labeled in Figure 5 (as well as Figures 8 and 10 for the other lateral

spreading sites) are approximated from post-event field and drone photos (Moug et al. 2023, SiteEye 2023) where available, and aerial imagery from Maxar (2023) dated February 12, 2023. Only features in the vicinity of the lateral spreading transects are represented. Flooding is not believed to have inundated this area on March 29, 2023 based on drone footage (A Haber 2023).

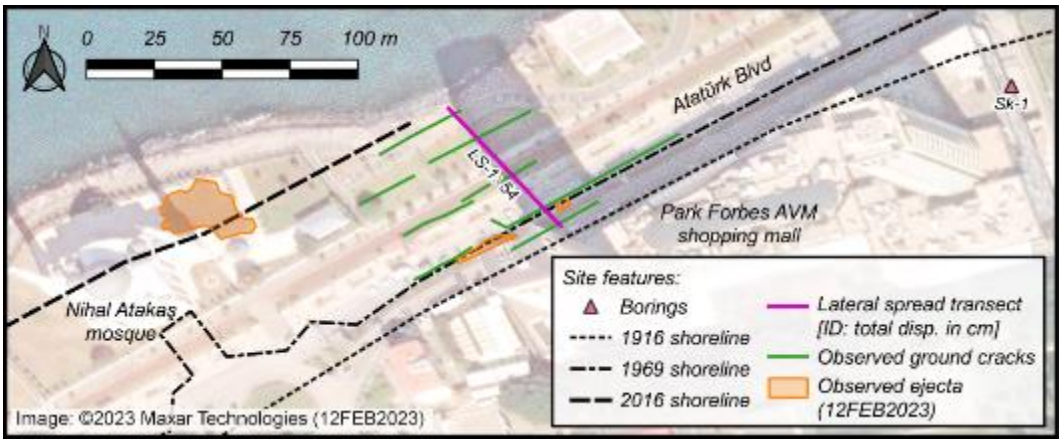

Figure 5. Map of lateral spreading site near the Nihal Atakaş mosque [background image obtained from Maxar (2023) is dated February 12, 2023].

Figure 6. Post-earthquake ground deformations observed near the Nihal Atakaş mosque: (a) sediment ejecta (36.5933N, 36.1574E; photo by Eylem Arslan taken February 14, 2023), and (b) lateral spreading along Atatürk Boulevard (36.5933N, 36.1594E; March 28, 2023).

Transect LS-1 measured on March 28, 2023 indicated a maximum lateral ground displacement of 54 cm over a distance of 65 m. It extended from a rubble mound seawall to the median of Atatürk Boulevard, in an area of post-1916 and pre-2016 reclaimed land. The seawall at this location appeared to be 0.5 to 0.8 m lower than the recently placed segment of seawall in front of the mosque; however, it was not clear whether this reduced seawall height existed before the earthquake. The overall extent of this spread to the south may have been constrained by the shopping mall structure.

The distribution of accumulated lateral displacement with distance from the shoreline along LS-1 is indicated in Figure 7a. The largest concentration of ground cracks (i.e., 20 cm movement over a 6 m distance) occurs within Atatürk Boulevard (Figure 6b) and coincides with the 1969 shoreline extent. However, the rate of accumulation of ground displacements otherwise remains relatively constant closer to the shore. LS-1 is only about 200 m west of boring Sk-1, which recorded a shallow ground water table depth of 1.5 m on April 20, 2010. Despite the absence of more detailed site data, it is likely the very loose to loose silty sands at depths below 4 m indicated in Sk-1 liquefied and contributed to the lateral spread.

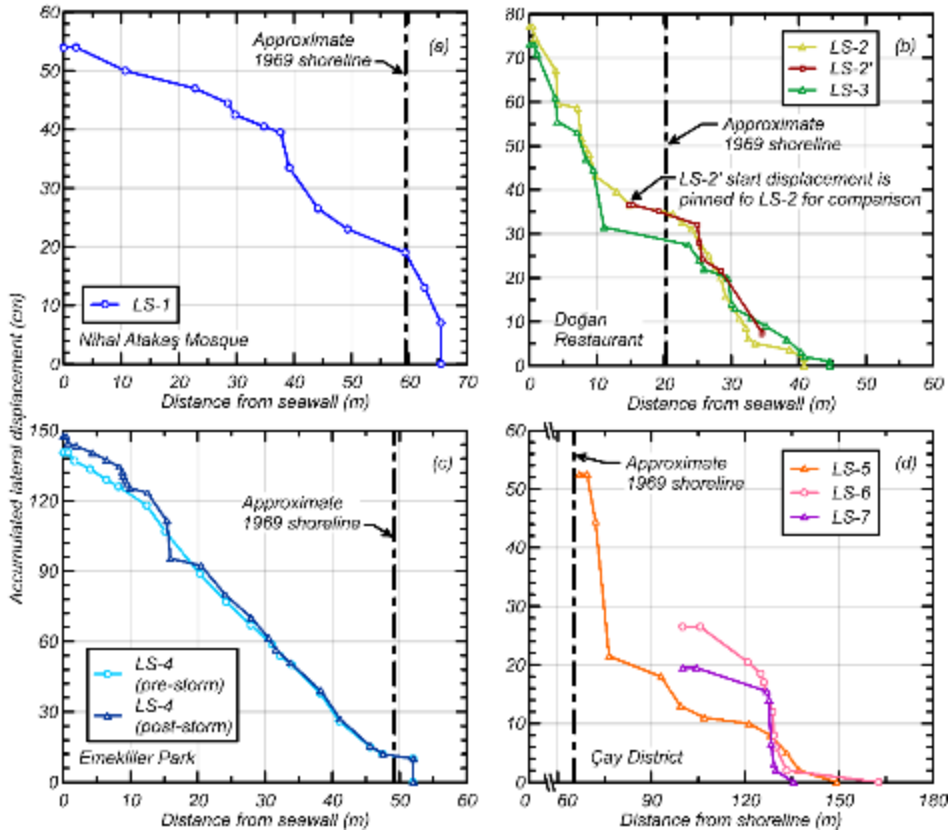

Figure 7. Accumulated lateral displacements relative to distance from the seawall (or shoreline) near (a) Nihal Atakaş mosque, (b) Doğan restaurant, (c) Emekliler Park, and (d) Çay District. The symbols indicate individual crack measurements that accumulate from the landward extent of the transect (where no movement is assumed). The approximate location of the 1969 shoreline is indicated. All transects are located within pre-1916 reclaimed fill.

Doğan Restaurant and Emekliler Park

The second lateral spreading case history site is located along the central shoreline of İskenderun, encompassing the Doğan restaurant facility (36.5934N, 36.1671E) and adjacent Emekliler Park area (36.5931N, 36.1682E) to the east (Figure 8). Several extensive ground

cracks were observed parallel to the shoreline between the seawall and Atatürk Boulevard (Figure 9a and 9d). The Teysir restaurant that had partially collapsed due to the March 29 storm surge is situated just east of the Emekliler park (Figure 8). A park bench situated along the shorefront walkway adjacent to the Doğan restaurant appeared stable during a reconnaissance visit on March 28, 2023, but had sunken into the ground following the March 29 storm surge and flood (Figure 9a). A one-story patio dining structure within the Doğan restaurant exhibited severe ground cracks through the floor and exterior walls (Figures 9b-c).

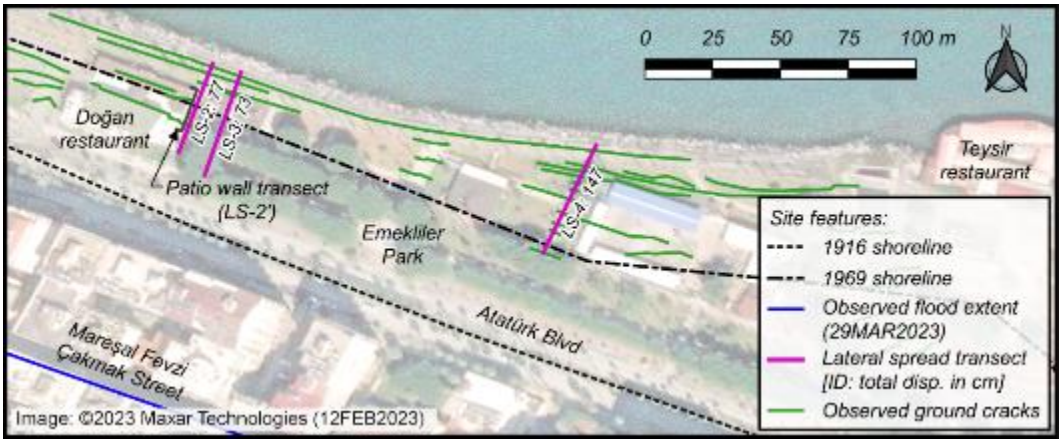

Figure 8. Map of lateral spreading site at the Doğan restaurant and Emekliler park [background image obtained from Maxar (2023) is dated February 12, 2023].

Figure 9. Lateral spreading at the Doğan restaurant and Emekliler park observed on April 1, 2023: (a) sunken park bench and shorefront damage behind Doğan restaurant patio (36.5936N, E36.1674E), (b) patio east exterior wall damage (36.5934N, 36.1672E), (c) patio damage (36.5935N, 36.1671E), and (d) transect LS-4 in Emekliler park (36.5930N, 36.1687E).

Transects LS-2 and LS-3 measured on April 1, 2023 indicated maximum lateral ground displacements of 77 cm and 73 cm over distances of 41 and 45 m, respectively. Both transects extended from the rubble mound seawall to the front (south side) of the Doğan restaurant. LS-2 was taken about 1 m away from the Doğan patio exterior walls, and LS-3 was taken 10 m to the east of LS-2. While both transects are within post-1916 reclaimed land, over half of the transect lengths are located seaward of the 1969 shoreline. The distribution of accumulated lateral displacements along LS-2 and LS-3 are depicted in Figure 7b to be consistent with each other. Slightly higher displacement rates (i.e., increased shear strain) along LS-2 and LS-3 were measured within 15 m from the seawall, which appears to coincide with post-1969 reclaimed fill.

Transect LS-2' only considered cracks along the base of the exterior patio wall and concrete fence of the Doğan restaurant (Figure 9b and right of Figure 9c). The cracks were measured over a limited distance from the north edge of the patio to the north edge of the two-story restaurant building. This transect was plotted in Figure 7b by matching the accumulated displacements at the northeast corner of the patio (i.e., 14.8 m from the seawall in LS-2). Cracks were concentrated with a total width of 10.5 cm along the column at the south edge of the patio (~25 m from the seawall), and a width of 14 cm at the north edge of the restaurant building (~28.5 m from the seawall). Despite these structurally controlled concentrations of cracks along the building, the total displacements along the extent of LS-2' approximately matched those along LS-2 and LS-3.

Transect LS-4 was measured in Emekliler park on March 28 and April 1, 2023 (before and after the March 29 storm) with respective maximum lateral ground displacements of 140 and 147 cm over the same distance of 52 m. The spread extended from the seawall to the southernmost crack observed, which coincides with the 1969 shoreline. The transect location was selected due to its location along a pedestrian pathway with concrete pavers that facilitated the measurement of extension cracks (Figure 9d). Figure 7c depicts a nearly constant rate of accumulated lateral displacements along the length of LS-4. This displacement rate approximately matches LS-2 and LS-3 within 15 m of the seawall. The inconsistency of the 1969 shoreline relative to the transects may indicate differences in subsurface soils (e.g., more newly placed fill) that would cause LS-4 to spread nearly twice as much as LS-2 and LS-3. Additionally, interpretation of the 1916 bathymetric depths of Figure 1, as presented in Table 2, suggest the seawall at LS-4 has an estimated free face

height range of 2.5 m to 5 m, whereas LS-2 and LS-3 have a lower estimated free face height range of 1.5 to 3.5 m. The measured increase in maximum displacements at LS-4 by 7 cm before and after the storm may have been due to scour and dislocation of surficial features (e.g., concrete pavers) during the storm, additional movements continuing since the earthquake or worsened by storm surge loading, measurement errors, or other effects.

Çay District

The third lateral spreading case history site (36.5907N, 36.1780E) is located in the Çay District east of the İskenderun city center, along a block of residential buildings (Figure 10). Significant sediment ejecta inundated Atatürk Boulevard in this area and was prevalent within the adjacent park and waterfront area in the hours immediately following the first M_w 7.8 mainshock (Cetin et al. 2023). Several of the buildings in the Çay District had settled by over 50 cm, as detailed in Moug et al. (2023) and Moug et al. (2024; in this special issue). A jetty and boat dock along the shorefront exhibited significant displacements and lateral spreading cracks (Figure 11a), and a wharf structure supporting a naval base to the east of the boat dock had collapsed during the earthquake.

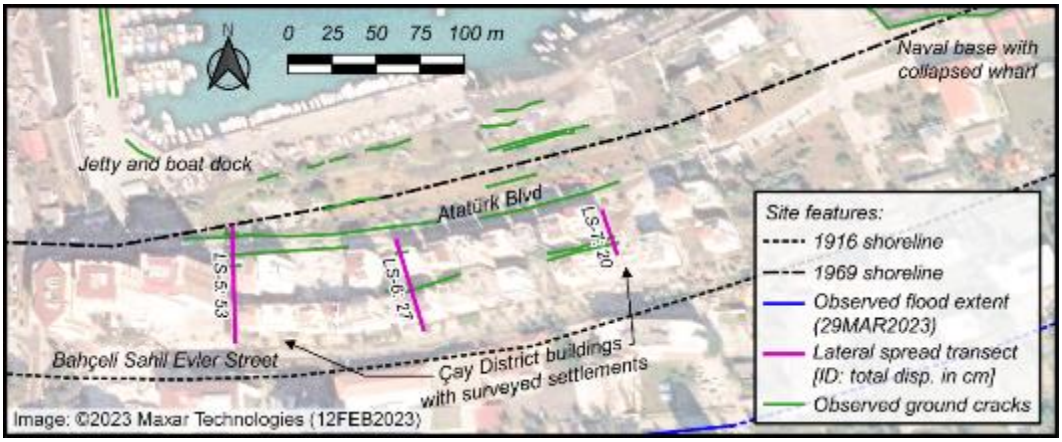

Figure 10. Map of lateral spreading site in the Çay District [background image obtained from Maxar (2023) is dated February 12, 2023]. While not visible here, significant ejecta was observed along Atatürk Boulevard in the hours after the earthquakes (Cetin et al. 2023).

Transects LS-5 (measured March 28), and LS-6 and LS-7 (measured April 1), indicated maximum lateral ground displacements of 53, 27, and 20 cm over distances of 82, 63, and 35 m, respectively. LS-5 extended from the north edge of Atatürk Boulevard (Figure 11b) to the north edge of Bahçeli Sahil Evler Street, LS-6 extended from the south edge of Atatürk Boulevard to the north edge of Bahçeli Sahil Evler Street, and LS-7 extended between the north edges of two 5-story structures. All three transects were located seaward of the

estimated 1916 shoreline but intersected the 1969 shoreline. Lateral spreading between the shoreline and the north edge of Atatürk Boulevard (i.e., 0 to ~100 m from the shoreline; Figure 7d) was not measured due to the low visibility of cracks within the lawn area and an inability to access the boat dock during these site visits. Over 50 cm of additional lateral displacement is believed to have occurred within this area based on a previous walkthrough (e.g., Figure 11a).

Figure 11. Post-earthquake ground deformations observed in the Çay District: (a) possible sand ejecta and lateral spreading near boat dock (36.5915N, 36.1789E; April 1, 2023), (b) cracks along Atatürk Blvd at the north end of transect LS-5 (36.5908N, 36.1767E; April 1, 2023), and (c) ground deformation and extensional cracks between settled buildings near LS-7 (36.5907N, 36.1792E; March 28, 2023).

Ground cracks were concentrated within the space between the two rows of 5-story buildings between Atatürk Boulevard and Bahçeli Sahil Evler Street (i.e., ~120 to 140 m from the shoreline; Figure 7d), suggesting over 20 cm of lateral extension in this area along LS-6 and LS-7 (Figure 11c). LS-5 depicted more gradual cracking between the buildings, which could potentially be attributed to a redistribution of crack patterns by a nearby 7-story building over a rigid foundation that had not settled. With the available information, it remains difficult to evaluate whether the cracks between the buildings resulted from ground deformation patterns influenced by building settlement (e.g., Moug et al. 2023; Figure 11c), overall seaward lateral spreading, or a combination of these or other mechanisms. Additional

insights from subsurface data, laser scan data, and computational analyses may help clarify the global picture of damage in this area.

REMOTE SENSING OBSERVATIONS

Interferometric Synthetic Aperture Radar (InSAR) is a powerful remote sensing technique that is now routinely used for studying earthquakes (e.g., Foumelis et al. 2021, Vassilakis et al. 2021). Recently, researchers have highlighted the contribution of InSAR products in mapping earthquake-induced secondary phenomena, such as soil liquefaction, lateral spreading, and landslides (e.g., Chatzipetros et al. 2021, Taftsoglou et al. 2023). Persistent Scatterer Interferometry (PSI) is an advanced interferometric technique applicable in monitoring ground deformation over time. PSI uses a large series of SAR imagery to measure subtle deformation signals, at a millimeter level of accuracy, on individual point targets named Persistent Scatterers (PS). PS are typically buildings, infrastructure, or surface features that remain stable over time. Although PSI has proven valuable mainly in applications related to land subsidence, rather than abrupt motions provoked by seismic events, it could be applied for the investigation of post-seismic deformation. Herein, PSI was considered to better understand the spatial and temporal patterns of the pre- and post-earthquake movements.

SAR Interferometric Data Analysis

PSI processing of İskenderun was based on two distinct time intervals, one prior to and the other following the February 6, 2023 earthquakes, to examine the effects of the earthquakes on ground deformation patterns. For the pre-seismic phase covering the period between January 2021 and January 2023, 136 Sentinel-1 (S-1) acquisition dates (descending track 021) were considered, while for the post-seismic period 14 S-1 (descending track 021) and 12 S-1 acquisition dates (ascending track 014) were used over the period between February and July 2023. For the post-seismic period, opposite acquisition geometries were used to constrain the east-west and vertical components of the deformation field along with their evolution in time.

For the interferometric processing of S-1 mission data, we used SNAPPING (Surface Motion Mapping) service (Foumelis et al. 2022) integrated on the Geohazards Exploitation Platform (GEP, https://geohazards-tep.eu). SNAPPING is an advanced multi-temporal SAR interferometric processor for the measurement of average surface motion rates and

corresponding displacement time series based on the PSI technique and Copernicus Sentinel-1 mission data.

For the interferometric analysis we followed a twofold processing scheme: (1) SNAPPING IFG for the generation and storage of an independent interferometric stack, and (2) SNAPPING PSI Med for time series analysis at medium resolution, using as inputs the previously stored interferometric stack. The conceptual model of SNAPPING processing is described in detail in Foumelis et al. (2022). For the SNAPPING PSI service, the removal of topographic components and geolocation were based solely on the SRTM 1 arc-second heights (NASA 2013). Furthermore, since there was no a priori knowledge of the stability of the area, the PSI solution was referenced to the average motion of the entire area. In this work, the PSI results correspond to the average Line of Sight (LOS) motion rate maps and displacement time series at a spatial sensor resolution of about 100 m.

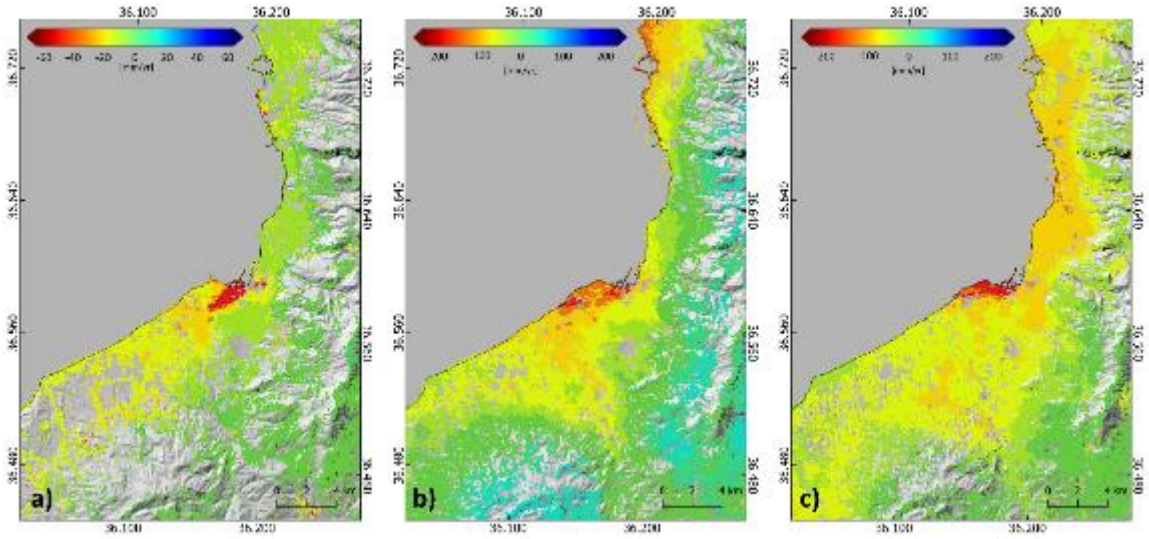

Figure 12. Sentinel-1 PSI LOS displacement rates for the regional area of İskenderun showing (a) pre-seismic period (Jan 2021-Jan 2023) of Descending orbit 21, (b) post-seismic period (Feb-July 2023) for the Descending orbit 21, and (c) post-seismic period (Feb-July 2023) for the Ascending orbit 014. The color scale is adjusted to the range of motion for each examined period.

SAR Results

Regional PSI deformation patterns before and after the earthquakes are shown in Figure 12. A change in the deformation pattern is clearly observed among the two periods. For the pre-seismic period (Jan 2021-Jan 2023), local subsidence is observed along the İskenderun harbor as well as within and to the south of the Çay District with rates reaching locally up to

5-6 cm/yr. The areas of highest subsidence appear to be centered near the historic alignment of the İbrahim Paşa channel (Figures 1-2). For the post-seismic period (Feb-Jul 2023), subsidence prevails throughout the shoreline and urban area with apparently increased rates of 20-30 cm/yr. However, the shorter post-earthquake monitoring period is influenced by seasonal biases relative to the two-year pre-earthquake monitoring period.

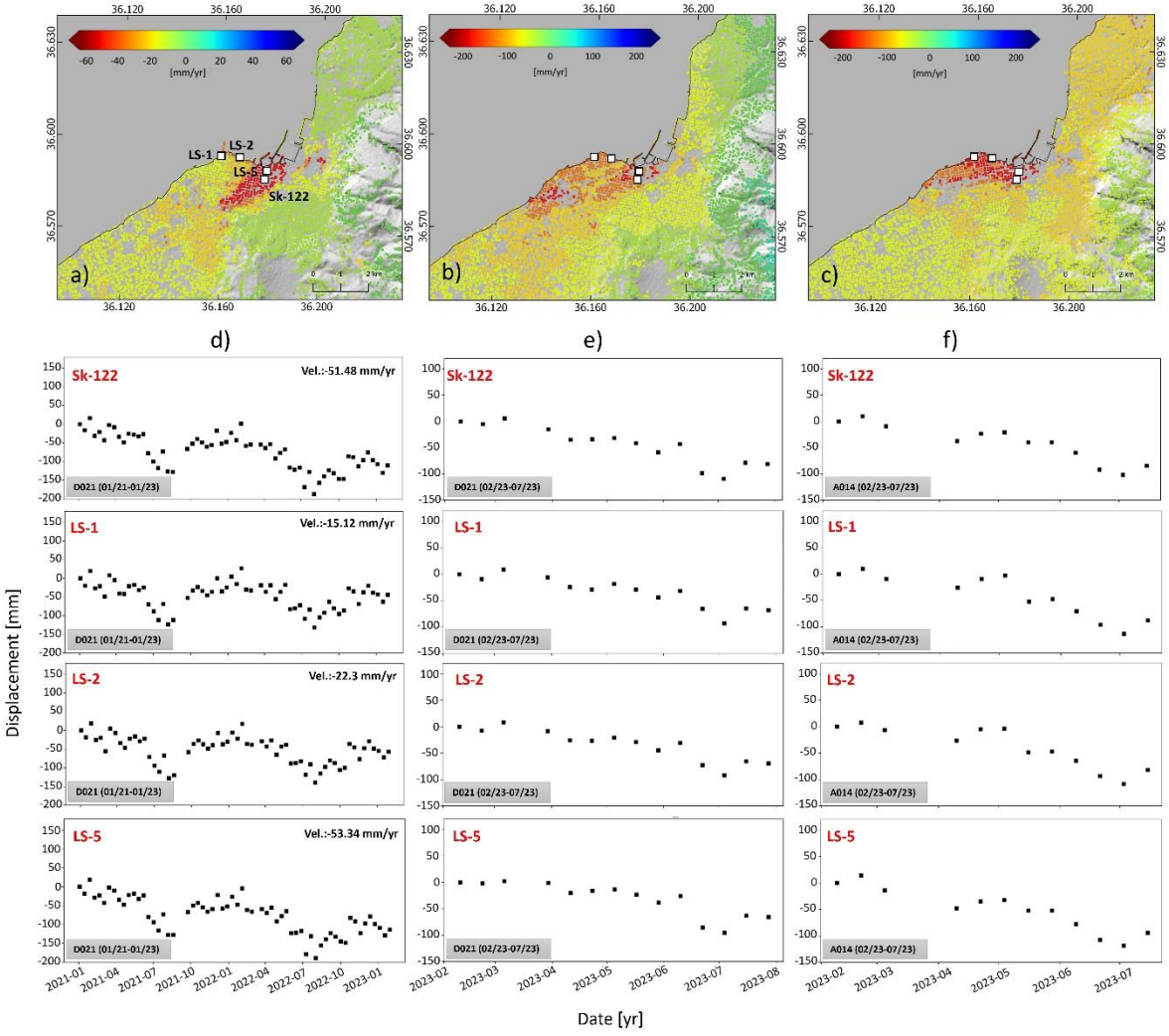

Figure 13. Sentinel-1 PSI LOS displacement rates for (a) pre-seismic period (Jan 2021-Jan 2023) for the Descending orbit 21, (b) post-seismic period (Feb-July 2023) for the Descending orbit 21, and (c) post-seismic period (Feb-July 2023) for the Ascending orbit 014. (d-f) Displacement time series respective to each geometry (a-c) for boring Sk-122, and lateral spreading transects LS-1, LS-2, and LS-5. The velocity value displayed on each time series plot is the least-squares fit of PSI data points for the timeline considered.

The time series analysis for selected sites near boring Sk-122, and lateral spread transects LS-1 (Nihal Atakaş mosque), LS-2 (Doğan restaurant), and LS-5 (Çay District) are indicated

in Figure 13. The deformations at these diverse locations follow a similar cyclic pattern characterized by seasonal variations. Over the two years of the pre-seismic observations, it appears that seasonal subsidence occurs during the summer period, and seasonal rebound occurs during the winter period when higher groundwater levels are expected. However, the areas experiencing the most significant subsidence do not fully rebound to the previous winter levels (e.g., sites Sk-122 and LS-5 in Figure 13d). Following the earthquake, the transition from winter to summer follows a similar seasonal subsidence trend suggesting that rapid post-earthquake ground movements over parts of the coastal area are partially influenced by the superimposition of the seasonal trend that cannot be quantitatively separated from the post-earthquake contribution.

To better isolate the post-earthquake contributions to subsidence, the InSAR analysis was reassessed for an approximately three-months period immediately following the earthquake (i.e., between February and April 2023), and compared to the same periods over the two years prior to the earthquake. The estimation of the motion rates for the period spanning from February to April, was performed by the recalculation of motion rates for the specific time span, as obtained from the full PSI time series solution. Figures 14a and 14b indicate that average displacements throughout İskenderun are typically under 5-7 cm/yr from February to April 2021, and February to April 2022. However, the results of Figure 14c indicate rapid subsidence of over 10-13 cm/yr on average in the majority of İskenderun after the earthquakes from February to April 2023. The greatest post-earthquake movements (up to 24 cm/yr) tend to be collocated with some of the observed liquefaction-induced ground deformations along the shoreline and in the Çay District area.

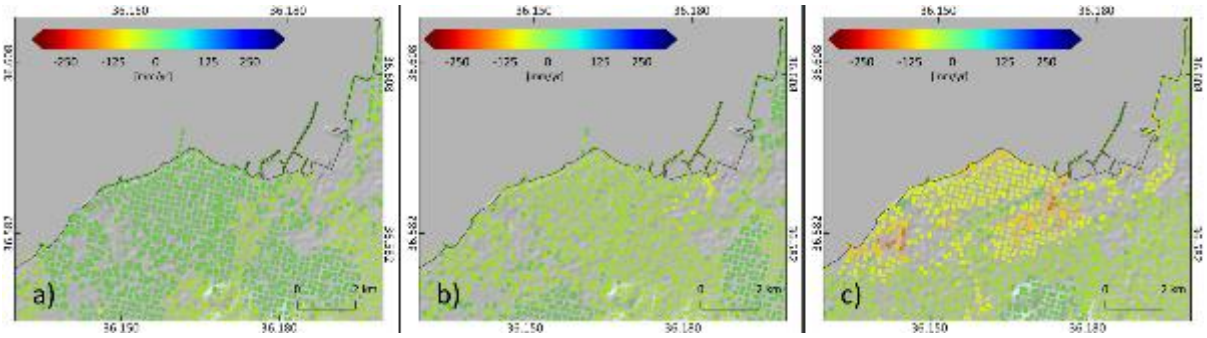

Figure 14. Sentinel-1 average PSI LOS displacement rates for the regional area of İskenderun showing the (a) pre-seismic period Feb-Apr 2021, (b) pre-seismic period Feb-Apr 2022, and (c) post-seismic period Feb-Apr 2023 of the Descending orbit 21.

The LOS measurements were decomposed into vertical and east-west motion components to facilitate the interpretation of subsidence and lateral deformation patterns. The vertical and east-west components were calculated using both ascending and descending Sentinel-1 geometries for the post-seismic period from February to April 2023. The procedure involved rasterization at 100 m of the PSI point vectors and combining the two components on common pixels. The PSI displacement field indicates that subsidence (Figure 15a) and lateral movements (Figure 15b) are largely concentrated within the İskenderun coastal area. The area along the first 2000 m of transects A-A' (Figure 15c) and B-B' (Figure 15d) typically indicate vertical subsidence rates of over 15 cm/yr. The highest rates of subsidence of 30 to 35 cm/yr are in the Çay District (Figure 15a,c; near borings Sk-13 and Sk-122). The highest eastward horizontal displacement rates of up to about 15 cm/yr are also located within the Çay District (Figure 15b), near the field surveyed lateral spreading transects LS-5, LS-6, and LS-7. The expectation of liquefaction-induced lateral spreading movements to occur perpendicular to and towards the shoreline is not apparent in Figure 15b due to the low sensitivity of this InSAR technique to north-south deformations. Furthermore, most lateral spreading displacements are believed to have occurred within the minutes or hours following the mainshock event. This short period is not captured by this analysis but may suggest slow continued lateral movements over the days and months following the mainshock.

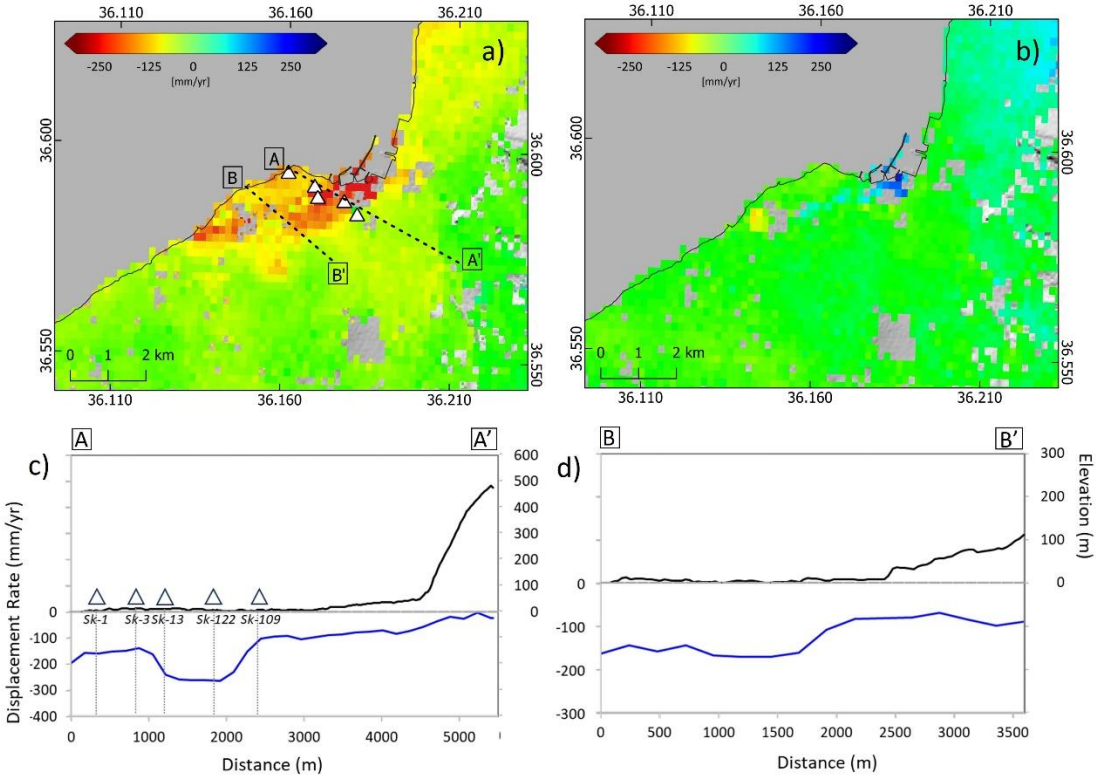

Figure 15. (a) Vertical and (b) east-west displacement rate maps of the study area for the Feb-Apr 2023 post-seismic period, decomposed from ascending and descending Sentinel-1 LOS observations. Profiles of vertical PSI motion and topography [SRTM 1 arc-second, (NASA 2013)] along transects (c) A-A' and (d) B-B'. Boring locations used in this study (Sk-1, -3, -13, -122, and -109) are shown in the rectangles.

DISCUSSION

The post-earthquake observations and remote sensing analyses herein provide insights for the severity and spatial distributions of liquefaction-induced ground deformations, pre- and post-earthquake ground subsidence, and recurrent floods. Together these details are indicative of the complex multi-hazard mechanisms affecting İskenderun.

An understanding of the early development of İskenderun and early shoreline extents indicate subsurface constraints potentially affecting the extents of liquefaction and lateral spreading. The case histories of lateral spreading herein follow patterns that suggest larger ground deformations occurred within more recently placed fills (i.e., post-1969; as opposed to fills placed prior to 1969). Liquefaction ground deformations affected several coastal communities during past earthquakes, particularly within areas of reclaimed land including the San Francisco shoreline in the 1989 Loma Prieta earthquake (e.g., Pease & O'Rourke 1997), and port and harbor facilities in the 1995 Kobe earthquake (e.g., Ishihara et al. 1996).

The lateral spreading case histories do not provide a direct measure of vertical subsidence relative to the sea level that would be expected to directly increase flood risks. Vertical subsidence is difficult to measure in the field in the absence of precise pre- and post-event elevation data. However, the magnitude and extent of lateral spreading observed along much of the İskenderun shoreline suggests a ubiquity of liquefiable sediments that volumetrically reconsolidated with the dissipation of pore pressures. This process is typically associated with vertical settlements that are of a similar magnitude as lateral spreading displacements at gently sloped sites (e.g., Holzer et al. 1999, Cetin et al. 2002). Evidence of reconsolidation settlements is further indicated by the large thickness of liquefaction susceptible soils in nearby boring logs, and observations of localized settlements of several buildings near the shoreline (e.g., Moug et al. 2023). It is thus possible that liquefaction-induced reconsolidation caused general subsidence throughout the İskenderun urban area.

Both pre- and post-earthquake displacement rates from remote sensing are conspicuously about three times higher within the İskenderun coastal and urban areas relative to

surrounding areas (Figure 12). This suggests an underlying mechanism may be causing regional subsidence of İskenderun, irrespective of the earthquakes. This could be associated with long-term (i.e., creeping) settlements within marsh deposits near the İbrahim Paşa channel (Figures 1-2) since the early urban development of İskenderun in the 20th century (e.g., Nalça Kıssaboylu et al. 2023), groundwater depletion, and other factors. Such ongoing subsidence likely worsened the flood hazard and may suggest why the flood extent observed on March 29, 2023 surpassed the observed extent of liquefaction-induced ground deformations (Figure 2).

Over the same three-months period (i.e., February to April), average pre-earthquake movements in İskenderun in 2021 and 2022 (Figures 14a-b) were approximately doubled following the earthquakes in 2023 (Figure 14c). Furthermore, the largest post-earthquake movements were generally located near observed liquefaction manifestations (Figure 2). While InSAR PSI methods can capture long-term (i.e., creeping) deformations with high certainty, the frequency of readings (i.e., every ~12 days) limits their ability to track short-term liquefaction-induced activity. Observations of liquefaction-induced sediment ejecta in past earthquakes (e.g., Ambraseys and Sarma 1969) and during the mainshock of the Kahramanmaraş earthquake sequence (e.g., Cetin et al. 2023) suggest that the majority of pore pressure dissipation and reconsolidation typically occurs within several minutes to hours after shaking ends. However, low permeability layers may greatly slow the reconsolidation of deeper liquefiable layers (e.g., Bassal and Boulanger 2021). Such a condition may suggest why boring Sk-122, with a 4-m thick clay crust and loose silty sand to depths of over 30 m is collocated with some of the highest post-earthquake subsidence rates of over 30 to 35 cm/yr (Figure 15c). More detailed studies will be needed to further confirm the cause of an increased post-earthquake subsidence rate.

Several other factors likely contributed to increased flooding risks in İskenderun. The proliferation of ejected sediments and pore fluids, and an increase in the ground water table induced by liquefaction (e.g., Davis et al. 2015) likely contributed to flooding soon after the mainshock. Also, the loss of freeboard due to settlement of the seawall was unable to adequately inhibit coastal storm surge. The settlement and instability of the seawall may have similarly been initiated by liquefaction and lateral spreading within subsurface soils. Damage to the water drainage system (METU 2023, Cetin et al. 2023) and the ponding of water along pavement and other non-draining surfaces likely slowed the ability for water to recede

following each storm. These local infrastructure effects and other factors highlight the complex interplay between seismic and flood hazards.

Work is currently ongoing by the authors to develop coastal storm surge models to elucidate the sensitivity of flood extents relative to ground subsidence patterns. Subsurface investigations are also underway by the authors to better understand the ground conditions relative to liquefaction triggering and liquefaction-induced ground deformations.

CONCLUSIONS

Liquefaction-induced damage and ongoing flooding along the İskenderun shoreline was observed following the 2023 Kahramanmaraş earthquakes. The lateral spreading case histories at the Nihal Atakaş mosque, Doğan restaurant and Emekliler park, and Çay District suggest a concurrence of liquefaction ground deformation patterns with reclaimed shoreline fills. The observed flooding due to coastal storm surge on March 29, 2023 typically surpassed the extent of observed liquefaction ground deformations. Remote sensing observations before and following the earthquakes suggest that long-term regional subsidence has been conspicuously occurring within İskenderun at a higher rate relative to surrounding areas. The remote sensing observations also suggest an accelerated rate of subsidence following the earthquakes, particularly near areas with liquefaction manifestations and post-earthquake flooding. Earthquake damage to shoreline protection structures and drainage systems, among other factors, likely also contributed to the flood hazard. This work highlights the importance of cross-disciplinary perspectives for evaluating the interdependence of liquefaction and flood hazards.

DECLARATION OF CONFLICTING INTERESTS

The author(s) declared no potential conflicts of interest with respect to the research, authorship, and/or publication of this article.

DATA AND RESOURCES

Some or all of the reconnaissance data disseminated in this work has been made available by the GEER association (https://geerassociation.org/), the data report by Moug et al. (2023), and the SiteEye Geo-Reconnaissance portal (https://app.sahagozu.com/). WorldView imagery was accessed through Maxar's Open Data Program (https://www.maxar.com/open-data/turkey-earthquake-2023). Sentinel-1 and Sentinel-2 imagery was obtained from the Copernicus Open Access Hub (https://scihub.copernicus.eu/). Data processing was performed

using the SNAP and SNAPPING services in the Geohazards Exploitation Platform (https://geohazards-tep.eu).

ACKNOWLEDGEMENTS

The work of the GEER Association is supported in part by the National Science Foundation (NSF) through the Engineering for Civil Infrastructure Program under Grant No. CMMI-1826118. Any opinions, findings, and conclusions or recommendations expressed in this material are those of the authors and do not necessarily reflect the views of the NSF. Any use of trade, firm, or product names is for descriptive purposes only and does not imply endorsement by the U.S. Government. The GEER Association is made possible by the vision and support of the NSF Geotechnical Engineering Program Directors: Dr. Giovanna Biscontin, Dr. Richard Fragaszy, and the late Dr. Cliff Astill. Researchers from the Middle East Technical University received support from the Turkish government. Additionally, Zemin Etüd vs Tasarim A.Ş. provided financial support for a team member. The authors are grateful for the support of Dr. H. Turan Durgunoğlu (ZETAS), Dr. Robb Moss (Cal Poly, SLO), Dr. Jorge Macedo (Georgia Tech), Dr. Halil Sezen (The Ohio State University), Dr. Michael Foumelis (Aristotle University of Thessaloniki), Mr. Cody Arnold (Georgia Tech), and Mr. Ahmet Palalıoğlu.

REFERENCES

A Haber (2023). “Hatay İskenderun'da deniz taştı yollar su altında kaldı!” [Video]. YouTube. Posted March 30, 2023. https://www.youtube.com/watch?v=Zo3ho0KQiIw&list=LL&index=2

Aksu, A. E., Calon, T. J., Hall, J., & Yaşar, D. (2005). “Origin and evolution of the Neogene İskenderun Basin, northeastern Mediterranean Sea.” Mar. Geol., 221, pp. 101-133, 10.1016/j.margeo.2005.03.011.

Aksu, A. E., Calon, T. J., Piper, D. J. W., Turgut, S., & Izdar, E. K. (1992). “Architecture of late orogenic basins in the eastern Mediterranean Sea.” Tectonophysics, 210 (1992), pp. 191-213.

Ambraseys, N. N. (1989). “Temporary seismic quiescence: SE Turkey.” *Geophysical Journal International*, 96(2), 311-331.

Ambraseys, N., & Sarma, S. (1969). “Liquefaction of soils induced by earthquakes.” Bull. Seismol. Soc. Am. 59 (2): 651–664. https://doi.org/10.1785/BSSA0590020651.

Atwater, B.F. (1987). “Evidence for great Holocene earthquakes along the outer coast of Washington State.” Science. v. 236, p. 942-944.

Bassal, P. C., & Boulanger, R. W. (2021). “System Response of an Interlayered Deposit with Spatially Preferential Liquefaction Manifestations.” Journal of Geotechnical and Geoenvironmental Engineering. ASCE, 147(12): https://doi.org/10.1061/(ASCE)GT.1943-5606.0002684.

Boulanger, R. W., & Idriss, I. M. (2015): CPT-based liquefaction triggering procedure. Journal of Geotechnical and Geoenvironmental Engineering, 142(2), 04015065, 10.1061/(ASCE)GT.1943-5606.0001388.

Boulanger, R. W., & Idriss, I. M. (2012). "Probabilistic SPT-based liquefaction triggering procedure." J. of Geotech. and Geoenviron. Engineering, ASCE, 138(10), 1185-1195, 10.1061/(ASCE)GT.1943-5606.0000700.

Buckreis, T., B. Güryuva, A. İçen, O. Okcu, A. Altindal, M. Aydin, R. Pretell, A. Sandikkaya, O. Kale, A. Askan, S. Brandenberg, T. Kishida, S. Akkar, Y. Bozorgnia, J. Stewart (2023) "Ground Motion Data from the 2023 Türkiye-Syria Earthquake Sequence." DesignSafe-CI. https://doi.org/10.17603/ds2-t115-bk16 v4.

Cetin, K. Ö., Bray, J. D., Frost, J. D., Hortacsu, A., Miranda, E., Moss, R. E. S., Stewart, J. P., et al. (2023). "February 6, 2023 Turkiye Earthquakes: Report on Geoscience and Engineering Impacts." Earthquake Engineering Research Institute, LFE Program, GEER Association Report 082, May 6, 2023. https://10.18118/G6PM34.

Cetin, K. O., Youd, T. L., Seed, R. B., Bray, J. D., Sancio, R., Lettis, W., Yilmaz, M. T., & Durgunoglu, H. T. (2002). "Liquefaction-induced ground deformations at Hotel Sapanca during Kocaeli (Izmit), Turkey earthquake." Soil Dyn and Earthquake Engr, 22, 1083–1092.

Cetin, K. O., Youd, T. L., Seed, R. B., Bray, J. D., Stewart, J. P., Durgunoglu, H. T., Lettis, W., & Yilmaz, M. T. (2004). "Liquefaction-Induced Lateral Spreading at Izmit Bay During the Kocaeli (Izmit)-Turkey Earthquake." J. of Geotech. and Geoenviron. Engineering, Vol. 130, No. 12. 10.1061/(ASCE)1090-0241(2004)130:12(1300).

Chatzipetros, A.; Pavlides, S.; Foumelis, M.; Sboras, S.; Galanakis, D.; Pikridas, C.; Bitharis, S.; Kremastas, E.; Chatziioannou, A.; Papaioannou, I. The northern Thessaly strong earthquakes of March 3 and 4, 2021, and their neotectonic setting. Bull. Geol. Soc. Greece 2021, 58, 222–255.

Darienzo, M. E., & Peterson, C. D. (1990). "Episodic tectonic subsidence of late Holocene salt marsh sequences in Netarts Bay, Oregon, central Cascadia margin, U.S.A.." Tectonics, v. 9, p. 1-22.

Davis, C. A., Giovinazzi, S., & Hart, D. E. (2015). "Liquefaction Induced Flooding in Christchurch, New Zealand." Proc., 6th Int. Conf. on Earthquake Geotechnical Engineering, Christchurch, New Zealand.

Holzer, T. L., Bennett, M. J., Ponti, D. J., & Tinsley III, J. C. (1999). "Liquefaction and Soil Failure during 1994 Northridge Earthquake." J. of Geotech. and Geoenviron. Eng., 125(6), 438–452. https://doi.org/10.1061/(ASCE)1090-0241

Flanders Marine Institute (VLIZ) and Intergovernmental Oceanographic Commission (IOC) (2023). "Sea level station monitoring facility." Accessed at https://www.ioc-sealevelmonitoring.org on 2023-09-18 at VLIZ. DOI: 10.14284/482

711 Foumelis, M., Delgado Blasco, J.M., Brito, F., Pacini, F., Papageorgiou, E., Pishehvar, P., & Bally, P.
712 (2022). “SNAPPING Services on the Geohazards Exploitation Platform for Copernicus Sentinel-
713 1 Surface Motion Mapping.” Remote Sens. 2022, 14, 6075. https://doi.org/10.3390/rs14236075.
714 Foumelis, M., Papazachos, C., Papadimitriou, E., Karakostas, V., Ampatzidis, D., Moschopoulos, G.,
715 Kostoglou, A., Ilieva, M., Minos-Minopoulos, D., Mouratidis, A., Kkallas, C., Chatzipetros, A.,
716 (2021). “On Rapid Multidisciplinary Response Aspects for Samos 2020 M7.0 Earthquake.” Acta
717 Geophysica, https://doi.org/10.1007/s11600-021-00578-6.
718 Google (2022). [Google street view imagery of Iskenderun shoreline dated January 2022; uploaded by
719 user Makro 360]. Retrieved September 1, 2023.
720 Goldberg, D. E., T. Taymaz, N. G. Reitman, A. E. Hatem, S. Yolsal-Çevikbilen, W. D. Barnhart, T.
721 S. Irmak, D. J. Wald, T. Öcalan, W. L. Yeck, et al. (2023). “Rapid Characterization of the
722 February 2023 Kahramanmaraş, Türkiye, Earthquake Sequence.” The Seismic Record. 3(2),156–
723 167, doi: 10.1785/0320230009.
724 Hughes, M. W., Quigley, M. C., van Ballegooy, S., Deam, B. L., Bradley, B. A., Hart, D. E., &
725 Measures, R. (2015). “The sinking city: Earthquakes increase flood hazard in Christchurch, New
726 Zealand.” GSA Today, v. 25, no. 3–4, doi: 10.1130/GSATG221A.1.
727 Ishihara, K. (2003). “Characteristics of Waterfront Landslides Induced by Earthquakes.” Proc. of Int.
728 Conf. on Fast Slope Movements-Prediction and Prevention for Risk Mitigation, Naples, Italy.
729 Ishihara, K., Yasuda, S., & Nagase, H. (1996). "Soil characteristics and ground damage." Special
730 Issue on Geotech. Aspects of the Jan 17, 1995 Hyogoken-Nambu Earthquake.” Soils and
731 Foundations, JGS, Jan., 109-118.
732 Lemke, R. W. (1967). “Effects of the Earthquake of March 27, 1964, at Seward, Alaska.” U. S.
733 Geological Survey Professional Paper 542-E, 43 p.
734 Mai, P. M., T. Aspiotis, T. A. Aquib, E. V. Cano, D. Castro-Cruz, A. Espindola-Carmona, B. Li, X.
735 Li, J. Liu, R. Matrau, et al. (2023). “The Destructive Earthquake Doublet of 6 February 2023 in
736 South-Central Türkiye and Northwestern Syria: Initial Observations and Analyses.” The Seismic
737 Record. 3(2), 105–115, doi: 10.1785/0320230007.
738 Maxar Technologies (Maxar) (2023). “Imagery Basemap, Catalog ID: 10300100E1B9D900,
739 Quadkey: 031133021303, Satellite: WV02, Collection date: Feb 12, 2023, 12:16:32-08:00.”
740 <maxar.com/open-data/turkey-earthquake-2023>
741 Maxar Technologies (Maxar) (2016). Imagery Basemap accessed via Google Earth on Sep 15, 2023,
742 Collection date: Nov 16, 2016.”
743 Middle East Technical University (METU) (2023). “Preliminary Reconnaissance Report on February
744 6, 2023, Pazarcık Mw=7.7 and Elbistan Mw=7.6, Kahramanmaraş-Türkiye Earthquakes.” Report
745 No. METU/EERC 2023-01, 20 February.

Moug, D., Bassal, P., Bray, J.D., Cetin, K.Ö., Kendir, S.B., Sahin, A., Cakir, El., Soylemez, B., and Ocak, S. (2023). “February 6, 2023 Turkiye Earthquakes: GEER Phase 3 Team Report on Selected Geotechnical Engineering Effects.” GEER Association Report 082-S1, June 30, 2023. https://doi.org/10.18118/G6F379.

Moug, D.M., Bray, J.D., Bassal, P., Macedo, J., Ulmer, K., Cetin, K.O., Kendir, S.B., Şahin, A., Arnold, C., & Bikçe, M (2024). "Liquefaction-Induced Building and Ground Interactions in İskenderun from the 2023 Kahramanmaraş Earthquake Sequence.” Earthquake Spectra, 87552930241232994 (in this issue).

Nalça, C. (2018). “Transformation of İskenderun Historic Urban Fabric from Mid 19th Century to the End of the French Mandate Period.” MS Thesis, Department of Architectural Restoration, İzmir Institute of Technology.

Nalça Kıssaboylu, C., Kul, F. N., & Rıfaioğlu, M. N. (2023). “Defining the Impacts of Historical Development Activities on Urban Heritage of İskenderun (Alexandretta).” ICONARP International Journal of Architecture and Planning, 11 (1),66-87. DOI: 10.15320./ICONARP.2023.233.

NASA Shuttle Radar Topography Mission (SRTM) (2013). “Shuttle Radar Topography Mission (SRTM) Global. Distributed by Open Topography.” https://doi.org/10.5069/G9445JDF. Accessed: 2023-09-08.

Orukoğlu, N. & İşhani, S. S. (2010). “Hatay Province, İskenderun District, İskenderun Municipality, Microzonation Study Report.” Denge Engineering Ltd., Antakya, Turkey.

Ozener, P., Monkul, M. M., Bayat, E. E., Ari, A., Cetin, K. O. (2024). “Liquefaction and performance of foundation systems in Iskenderun during 2023 Kahramanmaras-Turkiye earthquake sequence.” Soil Dynamics and Earthquake Engineering, 178 (2024) 108433, https://doi.org/10.1016/j.soildyn.2023.108433.

Özdemır, A., Yaşar, E., & Şahınoğlu, A. (2019). “Geothermal Geophysical Studies in İskenderun (Hatay): The First Indication for Geothermal Energy.” Proceedings of the 3rd International Symposium on Multidisciplinary Studies and Innovative Technologies, Ankara, Turkey.

Pease, J. W., & O’Rourke, T. D. (1997). “Seismic Response of Liquefaction Sites.” Journal of Geotech. and Geoenviron. Eng., 123(1), 37–45. https://doi.org/10.1061/(asce)1090-0241(1997)123:1(37).

Reitman, N. G., Briggs, R. W., Barnhart, W. D., Thompson, J. A., DuRoss, C. B., Hatem, A. E., Gold, R. D., Akçiz, S., Koehler, R. D., Mejstrik, J. D., Collett, C. (2023). “Fault rupture mapping of the 6 February 2023 Kahramanmaraş, Türkiye, earthquake sequence from satellite data: U.S. Geological Survey data release, https://doi.org/10.5066/P985I7U2

Robinson, K., Cubrinovski, M., Kailey, P., Orense, R. (2010). “Field Measurements of Lateral Spreading following the 2010 Darfield Earthquake.” Proc., Ninth Pacific Conference on Earthquake Engineering Building an Earthquake-Resilient Society, Auckland, New Zealand.

SiteEye, Geo-Reconaissance. https://app.sahagozu.com/project/detail/529/viewer/4343. Retrieved August 22, 2023.

Soylu, R. [@ragipsoylu] (2023). “Sea level has risen in earthquake-hit city of Iskenderun, Turkey.” February 7, 2023. Tweet.

Taftsoglou, M., Valkaniotis, S., Papathanassiou, G., Karantanellis, E. (2023). “Satellite Imagery for Rapid Detection of Liquefaction Surface Manifestations: The Case Study of Türkiye-Syria 2023 Earthquakes. *Remote Sensing*, 15, 4190. https://doi.org/10.3390/rs15174190.

Ulu, U et al. (2002). “1:500,000 Scale, Geological Map of Turkey: Hatay.” General Directorate of Mineral Research and Exploration, Ankara, Turkey.

Vassilakis, E., Kaviris, G., Kapetanidis, V., Papageorgiou, E., Foumelis, M., Konsolaki, A., Petrakis, S., Evangelidis, C. Alexopoulos, J., Karastathis, V. Voulgaris, N. & Tselentis G-A. (2022). “The September 27th, 2021, earthquake in central Crete (Greece). Detailed analysis of the earthquake sequence and indications for contemporary arc-parallel extension at the Hellenic arc.” Applied Sciences, 12, 2815, https://doi.org/10.3390/app12062815.